Hindawi
International Transactions on Electrical Energy Systems
Volume 2022, Article ID 3771752, 19 pages
https://doi.org/10.1155/2022/3771752

Research Article

Power Control of a Grid-Connected Doubly Fed Induction Generator Using H∞ Control and Kalman Filter

Aboozar Mohammad Nezhad, Behrouz Tousi, and Farnaz Sabahi

Faculty of Electrical and Computer Engineering, Urmia University, Urmia, Iran

Correspondence should be addressed to Behrouz Tousi; b.tousi@urmia.ac.ir

Received 18 December 2021; Revised 15 August 2022; Accepted 23 August 2022; Published 3 October 2022

Academic Editor: Subrata Kumar Sarker

A new control method for a grid-connected doubly fed induction generator (DFIG) is proposed in this paper, which is robust against parametric uncertainty and measurement noise. In general, the DFIG controllers can be divided into two main groups: the rotor side converter (RSC) and the grid side converter (GSC) controllers. The parameters of a DFIG may deviate from their rated values due to the operating conditions. For this parametric uncertainty, a robust H_∞ vector control (VC) is employed using the complex sensitivity approach. The design of the RSC controller has been carried out using the vector control strategy, and instead of proportional-integral (PI) controllers, a designed robust controller is used. One of the steps in vector control is the extraction of the measured currents to be used in the control equations. If the currents are polluted with noise, the system control will be impaired. Thus, using a Kalman filter is suggested to solve this problem. The effectiveness of the proposed method is then investigated using extensive simulations under various conditions. The obtained results confirm the efficient performance and robustness of the presented controller with model and measurement uncertainties.

1. Introduction

In recent decades, the application of wind energy as one of the important renewable energy sources (RES) has increasingly been extended all over the world thanks to its economic feasibility, environmental adaptability, and pollution-free features. One of the widely used technologies in wind plants, which has obtained high popularity over recent years, is the DFIG, which is mainly used in variable speed wind turbines on account of their outstanding advantages compared to other machines. The most salient feature of this type of generator is that the rotor transfers about 30% of the generator's power output through power electronics converters. Therefore, these converters must be designed efficiently and cost-effectively. Today, with the developments in power electronics devices, exploiting advanced control methods for induction machines has considerably increased.

The main well-known control methods for DFIGs are categorized into two models: vector control and direct control. These two methods do not provide new concepts or methodologies for DFIGs. Still, to a certain extent, they are similar to the vector control and/or direct torque control methods applied to alternating current (AC) drives. However, they are extended for applying to DFIGs. By employing the vector control through the field-oriented stator flux method [1, 2] or the field-oriented stator voltage method [3, 4], the active and reactive powers are controlled independently. The PI controllers are used for implementing this method. The main drawback of the vector control with PI controllers is that the system performance is highly dependent on the adjustment of the PI controller parameters and the accuracy of the machine parameters, such as resistances and inductances of stator and rotor. Although some studies using vector control optimization [5], predictive function controller [6], and internal state controller [7, 8] have shown acceptable performance in comparison to the response of the PI controller, their implementation is very difficult in the case of considering their formulations. The power control of the system has been carried out using the fuzzy logic method [9]. Despite the satisfactory response

of this strategy, the errors in parameter estimations degrade the efficacy and performance of the system. The multifunction control is proposed to regulate the active and reactive power control and grid synchronization and generate the maximum power at different wind speeds with flexible reference power variation [10]. The essential characteristic of the multiple-function controller is the exclusion of PI controllers, flow ring, and switching table.

A direct power control (DPC) method is one of the strategies proffered to solve the mentioned problem [11]. However, the variable switching frequency is one of the shortcomings of this method. To solve the variable switching frequency problem, the switching vector was selected based on a switching table, and then the problem was optimized over time to reduce the oscillations of torque or active power and flux or reactive power [11]. Although this approach gives a constant switching frequency, it needs instantaneous complex calculations. Moreover, oscillation problems occur when the generator operates close to the synchronous speed. To solve the conventional DPC problems, new control strategies based on Neural-Network- and Neuro-Fuzzy-DPC are proposed for DFIG driven by wind turbine under variable wind profile [12].

The variation of the parameters causes the uncertainties in the DFIG model, which in turn prevents from meeting the control objectives of the system. It should be noted that, besides the mentioned variation, the presence of noise in the measurement is another factor causing uncertainty in the DFIG model. The measurement and the use of the measured values in the subsequent stages of the control system are among the most basic control stages in both vector control and direct control methods. If these measurements are noisy with uncertainty, the system's control will be impaired. The extended Kalman filter (EKF) method is applied to rotor power control of a DFIG in the case of having some failure with the current sensor [13]. First, the system modeling and the state-space model are obtained by selecting the rotor and stator currents as the state variables. The state-space model outputs in the EKF algorithm are considered active and reactive power of system. A discrete model of the EKF algorithm is applied to the system. The system is simulated by applying active and reactive power variations in the presence of measurement noise. The EKF algorithm is used to detect the active and reactive power dynamically. The system then proceeds in three modes: (1) Rotor Flow Sensor Noise, (2) Out-of-Range Measurements, and (3) Sensor Damage and Nonmeasurable Moments to Control Power in Sensor Inefficient Condition. The method mainly focuses on the rotor and ignores further discussion, and simulations are performed on the stator and the entire system.

Based on only simulation results [14], the velocity and position of the inductive generator rotor are estimated using both EKF and unscented Kalman filter (UKF) methods without discussing their advantages and disadvantages. In the mentioned study, both methods showed a relatively good tracking performance. The rotor speed and flux of the DFIG are estimated using EKF, where the simulation results show that the speed is estimated well, knowing that the flux is somehow noisy [15]. The Kalman EKF and UKF filters are used to estimate the dynamical variables of the DFIG [16]. In the simulated system, a DFIG is connected to one of the buses of a 40-bus system. The magnitude and phase angle of current and voltage of the bus connected to the generator is required for conducting system studies and local control. These quantities are collected via a phasor measurement unit (PMU) device. The system may experience some faults, or an estimate of the dynamic state of the system may be required. Thus, EKF and UKF filters have been used for this purpose [16]. The simulation results show that the UKF method outperforms the EKF in estimating the dynamic state.

Most of the mentioned approaches use the Kalman filter for the DFIG either for estimating the position of the rotor to eliminate the need for the position sensor, estimating the system's state parameters and variables in network studies, or detecting and correcting the errors of the current sensor. According to [5–17], the authors have not encountered when the parameters and the operating point of the machine have changed due to variations in temperature or magnetic saturation and what will be the robust control of the system in the presence of the model and measurement uncertainties. Besides, the investigations on how the system responds in this case have yet to be conducted. In this paper, a combination of the robust controller and Kalman filter is proposed to solve the model and measurement uncertainties.

In this paper, the H_∞ robust control method based on the complex sensitivity approach is proposed for DFIGs. Sliding mode and H∞ robust control strategies are selected and compared for different wind speed modes [18]. Then, the rotor speed and rotor current are set as control variables and discussed in the transient response and steady state of the system. It has been shown that the H_∞ controller has a more acceptable transient response compared to sliding mode, but it has a higher overshoot and longer settling time. The droop controller is developed using the H_∞ controller in a microgrid [19]. After applying demand changes, the voltage and frequency of the system are adjusted, and it is proven that the steady-state system has its stability after fault clearance. An H_∞ controller is designed to mitigate the small-frequency oscillations of the power grid with a DFIG [20]. The proposed controller shows robust performance against wind speed variations, but it has deteriorated when there are communication delays in the feedback signals. A robust intelligent controller is designed for power-sharing to counter the effects of nonlinearities in the model and uncertainties in the operating conditions [21]. Strategy can provide the desired performance under various uncertainties in operating conditions. A control approach for DFIG has been performed by the combination of Matrix Converter with reduced-order EKF and Model Predictive Control method [22]. Although using reduced-order EKF has eliminated the drawback of the Model Predictive Control method in perturbations, the inductance changes have not been discussed. Adaptive filtering and robust control have been introduced for frequency estimation and virtual inertia control [23]. The conventional inertia controller is not appropriate for DFIG in the presence of uncertainties. Thus, the H_∞ robust controller [23] develops the frequency control loop and the robust controller to improve the inertial

Table 1: Comparisons between the controllers.

Name of controller	Advantages	Limitations
Proposed controller	(i) Nominal performance (ii) Proper tracking (iii) Noise and perturbation attenuation (iv) Robust stability (v) Optimal state between VC with PI controller and conventional DPC	—
VC with PI controller	(i) Nominal performance (ii) Simplicity of structure	(i) Sensitive to PI controller parameters and the machine parameters (ii) Sensitive to measurement uncertainty
Conventional DPC	(i) High tracking nominal performance (ii) Almost robustness	(i) The maximum oscillation (ii) Variable switching frequency (iii) Sensitive to measurement uncertainty
Others controllers	(i) The robustness during uncertainties [24] (ii) The robustness against parametric variations and good performances [25] (iii) The robustness against parametric variations and good performances [26]	(i) Not checking measurement uncertainty (ii) Not checking parametric uncertainty [24]

response of the DFIG. An adaptive fuzzy fractional-order proportional-integral (FOPI) control system is proposed to improve the performance of a power grid-connected DFIG-based wind power conversion system [24]. The designed adaptive control system can provide robustness during uncertainties without effect on the power quality supplied to the electric power grid (EPG), but it has not been investigated about the change of machine parameter. A novel direct reactive power control strategy based on the three-level inverter topology (DRPC-3N) is proposed to improve the performance and robustness of a DFIG-based wind power plant system [25]. The DRPC-3N strategy provides robustness against parametric variations and good performances, which includes sinusoidal AC-generated current with low harmonic distortion and fewer ripples in the output, but it has not been investigated about the measurement uncertainties. A modulated hysteresis-direct reactive power control (MH-DRPC) strategy is designed to fix the switching frequency of the DFIG [26]. In this method, reactive power control-based fuzzy logic control and modulated hysteresis (MH) direct torque control are combined. The MH-DRPC strategy achieve sinusoidal forms of generated AC current with a constant frequency with minimal current total harmonic distortion and minimum output voltage ripple irrespective of the wind speed fluctuations and the robustness against parametric variations, but it has not been investigated about the measurement uncertainties. In contrast to [18–26] improving the performance of DFIG by using the H_∞ controller and other controllers, this paper intends to improve both the performance and the stability of the DFIG in the presence of both model and measurement uncertainties by proposing a new controller based on the combination of H_∞ controller method with the Kalman filter compared to the classical vector control. Table 1 shows the advantages and limitations of other control methods and the proposed method.

In the proposed method, we use the topology used in [27]. The method is different since, in the above-mentioned reference, an energy storage battery system is employed to reduce the oscillations of the injected power to the grid due to the wind variations, and the injected power is controlled in GSC. RSC operates through the PI controllers [27]. As mentioned before, vector control with PI controllers is susceptible to system parameters, and by deviating the parameters from their nominal value, the system's performance is reduced.

Both main methods (VC and DPC) of DFIG control have advantages and disadvantages. In such cases, it is necessary to use more advanced controls to stabilize and improve system performance against changes in system parameters and other system uncertainties. The purpose of this paper is to use a control method that, in addition to having a robust performance, has the advantages of the classical vector control method and its combination with a Kalman filter to eliminate measurement noise. In the proposed robust controller design, the mixed sensitivity method with a multiobjective cost function is used, and this function fulfills the design aim in nominal performance, proper tracking, perturbation attenuation, robust stability, and the designed system. In the case of uncertainties, system modeling and measurements have taken place, the power injected into the grid has been kept constant, and performance and stability have been achieved. The current study makes use of a robust H∞ controller in the current control loop of the RSC to make the system robust against the variations in the machine parameters. Also, given the fact that the measurements always are polluted with noise, the paper considers this problem and proposes a Kalman filter to alleviate the issue. The main contribution of this paper is to control the output power of DFIG and keep it constant in the case of adding the worst possible uncertainty to the system, compared to the classical vector control.

The rest of the paper is structured as follows: in Section 2, the DFIG model is introduced, and the design details of the robust H∞ controller method and Kalman filter are

described in Section 3 and Section 4, respectively. Then, the simulation results of the control method are illustrated in Section 5, which verifies the robustness and efficiency of the proposed controller with model and measurement uncertainties.

2. DFIG Model

2.1. Mathematical Model of DFIG. The descriptive equations related to the stator and rotor voltages in the synchronous reference frame are given as follows [28]:

$$V_{ds} = R_s.i_{ds} + \frac{d\lambda_{ds}}{dt} - \omega_s.\lambda_{qs}, \tag{1}$$

$$V_{qs} = R_s.i_{qs} + \frac{d\lambda_{qs}}{dt} + \omega_s.\lambda_{ds}, \tag{2}$$

$$V_{dr} = R_r.i_{dr} + \frac{d\lambda_{dr}}{dt} - (\omega_s - \omega_m).\lambda_{qr}, \tag{3}$$

$$V_{qr} = R_r.i_{qr} + \frac{d\lambda_{qr}}{dt} + (\omega_s - \omega_m).\lambda_{dr}. \tag{4}$$

Equations related to the stator and rotor fluxes are presented as

$$\lambda_{ds} = L_s i_{ds} + L_m i_{dr}, \tag{5}$$

$$\lambda_{qs} = L_s i_{qs} + L_m i_{qr}, \tag{6}$$

$$\lambda_{dr} = L_r i_{dr} + L_m i_{qs}, \tag{7}$$

$$\lambda_{qr} = L_r i_{qr} + L_m i_{qs}, \tag{8}$$

where V_{qs}, V_{ds}, V_{qr}, and V_{dr} are the stator and rotor voltages on q and d axes, i_{qs}, i_{ds}, i_{qr}, and i_{dr} are the stator and rotor currents on q and d axes, respectively. ω_s and ω_m are the synchronous and rotor speeds, respectively, and λ_{qs}, λ_{ds}, λ_{qr}, and λ_{dr} are the stator and rotor fluxes on q and d axes. R_s and R_r denote the stator and rotor resistances, and L_s and L_r are the self-inductances of the stator and rotor, where L_m is the mutual inductance.

The equations related to the active and reactive output power of the stator are written as

$$P_s = -\frac{3}{2}\left(V_{qs}i_{qs} + V_{ds}i_{ds}\right), \tag{9}$$

$$Q_s = -\frac{3}{2}\left(V_{qs}i_{ds} - V_{ds}i_{qs}\right). \tag{10}$$

2.2. State-Space Model. The state-space model of any given system, in general, is as follows [29]:

$$\dot{X} = [A]X + [B]U, \tag{11}$$

$$Y = [C]X + [D]U. \tag{12}$$

By defining the system state vector as $x = \begin{bmatrix} i_{dr} & i_{qr} & \lambda_{ds} & \lambda_{qs} \end{bmatrix}$, the input rotor voltage vector as $\mathbf{U}_r = \begin{bmatrix} \mathbf{V}_{dr} & \mathbf{V}_{qr} \end{bmatrix}^T$, the input stator voltage vector as $U_s = \begin{bmatrix} V_{ds} & V_{qs} \end{bmatrix}^T$, and the output vector as $Y = \begin{bmatrix} i_{dr} & i_{qr} & i_{ds} & i_{qs} \end{bmatrix}^T$, as well as considering equations (1)–(8), the state-space matrices can be written as follows:

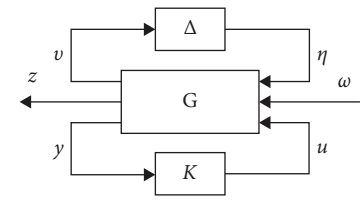

Figure 1: General framework of the problem of robust control.

$$A = \begin{bmatrix} -\left(\frac{a+1}{T_r} + \frac{a}{T_s}\right) & \omega_s - \omega_m & \frac{a}{L_m T_s} & -\frac{a\omega_m}{L_m} \\ -(\omega_s - \omega_m) & -\left(\frac{a+1}{T_r} + \frac{a}{T_s}\right) & \frac{a\omega_m}{L_m} & \frac{a}{L_m T_s} \\ \frac{L_m}{T_s} & 0 & -\frac{1}{T_s} & \omega_s \\ 0 & \frac{L_m}{T_s} & -\omega_s & -\frac{1}{T_s} \end{bmatrix}, \tag{13}$$

$$B_s = \begin{bmatrix} -\frac{a}{L_m} & 0 \\ 0 & -\frac{a}{L_m} \\ 1 & 0 \\ 0 & 1 \end{bmatrix} B_r = \begin{bmatrix} \frac{1}{\sigma L_r} & 0 \\ 0 & \frac{1}{\sigma L_r} \\ 0 & 0 \\ 0 & 0 \end{bmatrix} B = \begin{bmatrix} B_s & B_r \end{bmatrix}, \tag{14}$$

$$C = \begin{bmatrix} 1 & 0 & 0 & 0 \\ 0 & 1 & 0 & 0 \\ -\frac{L_m}{L_s} & 0 & \frac{1}{L_s} & 0 \\ 0 & -\frac{L_m}{L_s} & 0 & \frac{1}{L_s} \end{bmatrix}, \tag{15}$$

where $a = 1 - \sigma/\sigma$, $\sigma = 1 - L_m^2/L_s L_r$, $T_s = L_s/R_s$, and $T_r = L_r/R_r$.

3. Design of H_∞ Controller

The problem of robust control can be described [29] in Figure 1.

In Figure 1, G refers to the interconnection structure of the system, which includes the system's nominal model, the uncertainty weight function, and the performance weight function. Besides, K and Δ, respectively, refer to the designed

controller and the system's uncertainty matrix, whose model is extracted using the uncertainty type. To solve the problem of robust control, first, an uncertainty matrix must be extracted from the system, and then, according to the type of solution method and the purpose of the problem, the controller is designed. Here, H_∞ control is used in the procedure of the design of the controller.

There are various methods to implement H_∞ controllers in feedback design problems. It would be beneficial to have a standard formulation for a problem to be solved. The general structure of such a standard formulation [30] is shown in Figure 1.

The signals given in Figure 1 are described as follows: u shows control variables, y gives the measuring variables, w denotes external signals, such as disturbance and sensor noises, and z is the output that must be controlled, such as the tracking error. The H_∞ control aims to find a stable controller K, where the norm of H_∞ could minimize the transfer function from $w$to z.

The controller of a DFIG can be divided separately into RSC and GSC controllers. The methodology used is as follows. The RSC controller design has been carried out using the vector control strategy, and a designed robust controller will be used instead of PI controllers, which had been employed in classic vector controllers, to eliminate the drawbacks of classic vector control and avoid the disturbance of system performance due to changes in machine parameters, such as resistances and inductances of stator and rotor. The main objective of the RSC controller is to control the stator's active and reactive power. Based on the vector control method, stator active and reactive power can be controlled separately by controlling the rotor's q and d axes currents.

In designing the robust controller, uncertainty is considered a parametric uncertainty. The values of parameters with uncertainty are taken into account as [29–33]

$$R_s = \overline{R_S}\left(1 + k_{R_S}\delta_{R_S}\right), \tag{16}$$

$$\mathrm{R_r} = \overline{R_r}\left(1 + \mathrm{k_{R_r}}\delta_{\mathrm{R_r}}\right), \tag{17}$$

$$\omega_s = \overline{R_S}\left(1 + k_{\omega_s}\delta_{\omega_s}\right). \tag{18}$$

In the above equations, $\overline{R_S}$ and $\overline{R_r}$ are the rated values of stator and rotor resistances.k_{R_s}, k_{R_r}, and k_{ω_m} are uncertainty relationships with their corresponding parameters, and their values are 0.5, 0.5, and 0.3, respectively [34–36]. δ_{R_s}, δ_{R_r}, and δ_{ω_m} are any arbitrary numbers subject to $|\delta_{R_s}.\delta_{R_r}.\delta_{\omega_m}| \le 1$. By replacing these parameters in the system, the system model with uncertainty will be extracted. The equations are generally as follows [29–33]:

$$A = A_0 + A_{R_S}\delta_{R_S} + A_{R_r}\delta_{R_r} + A_{\omega_m}\delta_{\omega_m}, \tag{19}$$

$$B = B_0 + B_{R_S}\delta_{R_S} + B_{R_r}\delta_{R_r} + B_{\omega_m}\delta_{\omega_m}. \tag{20}$$

Since the uncertain parameters appear only in matrix A, the matrices related to the uncertain parameters of matrix B are zero. After calculations, the matrices of (19) and (20) become

$$A_0 = \begin{bmatrix} -\left(\frac{a+1}{\overline{T_r}} + \frac{a}{\overline{T_s}}\right) & 0 & \frac{a}{L_m\overline{T_s}} & -\frac{a\omega_s}{L_m} \\ 0 & -\left(\frac{a+1}{\overline{T_r}} + \frac{a}{\overline{T_s}}\right) & \frac{a\omega_s}{L_m} & \frac{a}{L_m\overline{T_s}} \\ \frac{L_m}{\overline{T_s}} & 0 & -\frac{1}{\overline{T_s}} & \omega_s \\ 0 & \frac{L_m}{\overline{T_s}} & -\omega_s & -\frac{1}{\overline{T_s}} \end{bmatrix}, B_0 = \begin{bmatrix} B_s & B_r \end{bmatrix}, \tag{21}$$

$$A_{R_s} = \begin{bmatrix} -\left(k_{R_s}\frac{a}{\overline{T_s}}\right) & 0 & k_{R_s}\frac{a}{L_m\overline{T_s}} & 0 \\ 0 & -\left(k_{R_s}\frac{a}{\overline{T_s}}\right) & 0 & k_{R_s}\frac{a}{L_m\overline{T_s}} \\ \frac{k_{R_s}L_m}{\overline{T_s}} & 0 & -\frac{k_{R_s}}{\overline{T_s}} & 0 \\ 0 & \frac{k_{R_s}L_m}{\overline{T_s}} & 0 & -\frac{k_{R_s}}{\overline{T_s}} \end{bmatrix}, B_{R_s} = 0, \tag{22}$$

$$A_{R_r} = \begin{bmatrix} -\left(k_{R_r}\frac{a+1}{\overline{T_r}}\right) & 0 & 0\,0 \\ 0 & -\left(k_{R_r}\frac{a+1}{\overline{T_r}}\right) & 0\,0 \\ 0 & 0 & 0\,0 \\ 0 & 0 & 0\,0 \end{bmatrix}, B_{R_r} = 0, \tag{23}$$

$$A_{\omega_m} = \begin{bmatrix} 0 & -K_{\omega_m}\omega_s & 0 & -\frac{aK_{\omega_m}\omega_s}{L_m} \\ K_{\omega_m}\omega_s & 0 & \frac{aK_{\omega_m}\omega_s}{L_m} & 0 \\ 0 & 0 & 0 & 0 \\ 0 & 0 & 0 & 0 \end{bmatrix}, B_{\omega_m} = 0, \tag{24}$$

where $\overline{T_s} = L_s/R_s$ and $\overline{T_r} = L_r/R_r$. By substituting (19) and (20) into the equation of the state variable (11) and rewriting, we will have

$$\begin{aligned} \dot{x} &= \left(A_0 + A_{R_S}\delta_{R_S} + A_{R_r}\delta_{R_r} + A_{\omega_m}\delta_{\omega_m}\right)x \\ &\quad + \left(B_0 + B_{R_S}\delta_{R_S} + B_{R_r}\delta_{R_r} + B_{\omega_m}\delta_{\omega_m}\right)u = \left(A_0 B_0\right)\begin{pmatrix} x \\ u \end{pmatrix} \\ &\quad + \delta_{R_S}\left(A_{R_S}B_{R_S}\right)\begin{pmatrix} x \\ u \end{pmatrix} + \delta_{R_r}\left(A_{R_S}B_{R_S}\right)\begin{pmatrix} x \\ u \end{pmatrix} \\ &\quad + \delta_{\omega_m}\left(A_{\omega_m}B_{\omega_m}\right)\begin{pmatrix} x \\ u \end{pmatrix} = \left(A_0 B_0\right)\begin{pmatrix} x \\ u \end{pmatrix} + \widetilde{W}_w, \end{aligned} \tag{25}$$

$$\widetilde{W}_w = \begin{bmatrix} \delta_{R_S}A_{R_S} & \delta_{R_S}B_{R_S} \\ \delta_{R_r}A_{R_r} & \delta_{R_r}B_{R_r} \\ \delta_{\omega_m}A_{\omega_s} & \delta_{\omega_m}B_{\omega_s} \end{bmatrix}\begin{bmatrix} x \\ u \end{bmatrix} = \widetilde{\Delta}_w\widetilde{Z}_w, \tag{26}$$

$$\widetilde{Z}_w = \begin{bmatrix} A_{R_S} & B_{R_S} \\ A_{R_r} & B_{R_r} \\ A_{\omega_s} & B_{\omega_s} \end{bmatrix} \begin{bmatrix} x \\ u \end{bmatrix}. \tag{27}$$

In the above equations, $\widetilde{W}_W$ and $\widetilde{Z}_W$ are, respectively, the input and output signals of the disturbance channel related to the uncertain parameter. Combining the state space of the system and the uncertainty model results in

$$\begin{bmatrix} \dot{x} \\ \widetilde{z}_w \\ y \end{bmatrix} = \begin{bmatrix} A_0 & I & B_0 \\ A_w & Z_{12} & B_w \\ C & Z_{2*12} & Z_{2*4} \end{bmatrix} \begin{bmatrix} x \\ \widetilde{w}_w \\ u \end{bmatrix}, \tag{28}$$

$$A_w = \begin{bmatrix} A_{R_S} \\ A_{R_r} \\ A_{\omega_m} \end{bmatrix}.B_w = \begin{bmatrix} B_{R_S} \\ B_{R_r} \\ B_{\omega_m} \end{bmatrix} = Z_{12*4}.I = \begin{bmatrix} I_4 & I_4 & I_4 \end{bmatrix}, \tag{29}$$

$$\widetilde{W}_w = \widetilde{\Delta}_w \widetilde{Z}_w.\widetilde{\Delta}_w = \begin{bmatrix} \delta_{R_s} I_4 & Z_4 & Z_4 \\ Z_4 & \delta_{R_r} I_4 & Z_4 \\ Z_4 & Z_4 & \delta_{\omega_m} I_4 \end{bmatrix}. \tag{30}$$

Here, I_i is the i-dimensional identity matrix, Z_I is the i-dimensional zero matrices, and Zi*j is the zero matrices with i number of rows and j number of columns. Since the elements of the two last matrices A_{R_r} A_{ω_m} are zero, (28) can be rewritten as

$$\begin{bmatrix} \dot{x} \\ z_w \\ y \end{bmatrix} = \begin{bmatrix} A_0 & I_{new} & B_0 \\ C_w & Z_8 & D_w \\ C & Z_{2*8} & Z_{2*4} \end{bmatrix} \begin{bmatrix} x \\ w_w \\ u \end{bmatrix}, \tag{31}$$

$$W_w = \Delta_w Z_w.\Delta_w = \begin{bmatrix} \delta_{R_s} I_4 & Z_{4*2} & Z_{4*2} \\ Z_{2*4} & \delta_{R_r} I_2 & Z_{2*2} \\ Z_{2*4} & Z_{2*2} & \delta_{\omega_m} I_2 \end{bmatrix}, \tag{32}$$

$$C_w = \begin{bmatrix} C_{R_s} \\ C_{R_r} \\ C_{\omega_m} \end{bmatrix}.D_w = Z_{8*4}.I_{new} = \begin{bmatrix} [I_4] & \begin{bmatrix} I_2 \\ Z_2 \end{bmatrix} & \begin{bmatrix} I_2 \\ Z_2 \end{bmatrix} \end{bmatrix}, \tag{33}$$

$$C_{R_r} = \begin{bmatrix} -\left(k_{R_r} \dfrac{a+1}{\overline{T}_r}\right) & 0 & 0 & 0 \\ 0 & -\left(k_{R_r} \dfrac{a+1}{\overline{T}_r}\right) & 0 & 0 \end{bmatrix}, \tag{34}$$

$$C_{\omega_m} = \begin{bmatrix} 0 & -K_{\omega_m}\omega_s & 0 & -\dfrac{aK_{\omega_m}\omega_s}{L_m} \\ -K_{\omega_m}\omega_s & 0 & \dfrac{aK_{\omega_m}\omega_s}{L_m} & 0 \end{bmatrix}. \tag{35}$$

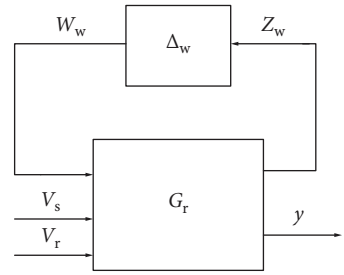

Figure 2: Representation of system LFT.

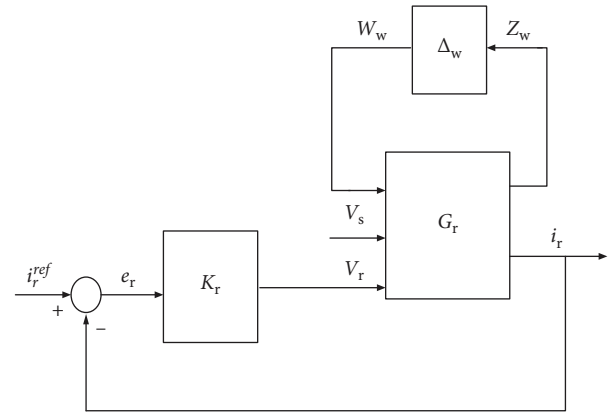

Figure 3: Closed-loop structure of the designed system.

G_r is the realization of the state-space (31), which can be presented as follows:

$$G_r = \begin{bmatrix} A_r & B_r \\ C_r & D_r \end{bmatrix}, \tag{36}$$

$$A_r = A_0.B_r = [I_{\text{new}} B_0]. = \begin{bmatrix} C_w \\ C \end{bmatrix}.D_r = Z_{10*12}. \tag{37}$$

The representation of the system with uncertainty besides the linear fractional transformations (LFT) transform is given in Figure 2.

By representing system LFT, a standard control structure for establishing the H_∞ controller can be obtained, as shown in Figure 3.

Here, the H_∞ controller with a complex sensitivity formation is used [29, 30]. The interconnections of the system for obtaining a controller with the utilized complex sensitivity approach are shown in Figure 4. $W_r = [V_{ds} V_{qs} i_{dr}^{\text{ref}} i_{qr}^{\text{ref}}]^T$ is the external control input, which includes stator voltages and rotor reference currents, $u = V_r = \begin{bmatrix} V_{dr} & V_{qr} \end{bmatrix}^T$ is the controller output, $e_r = [e_{dr} e_{qr}]^T = [i_{dr}^{\text{ref}} - i_{dr} i_{qr}^{\text{ref}} - i_{qr}]^T$ is the controller input, which is equal to the tracking error, and $i_r = [i_{dr} i_{qr}]^T$ is the measurement matrix of outputs. Signal z includes all controlled signals and tracking errors.

A standard solution for the H∞ control problem is to find a controller where the H∞ norm minimizes the transfer function from Wr to Zr, the resultant value must be at least

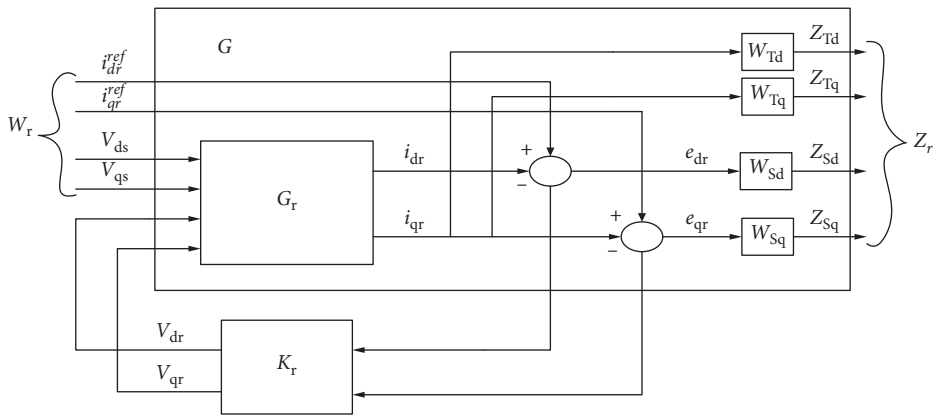

Figure 4: System interconnections.

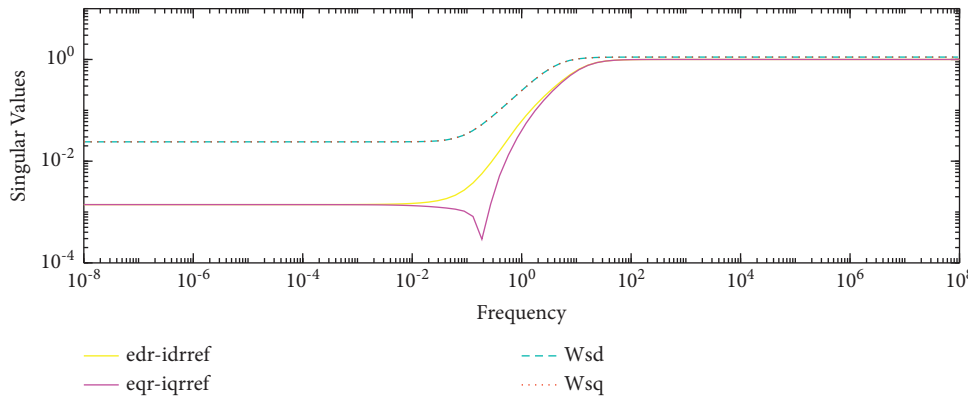

Figure 5: The sensitivity function and the inverse of the weighted performance function.

smaller than the unit to ensure system stability (according to the small gain theorem), and its definition by using the complex sensitivity approach is [30, 31]

$$\left\| \begin{matrix} W_S(I + G_r K_r)^{-1} \\ W_T G_r K_r * (I + G_r K_r)^{-1} \end{matrix} \right\|_\infty \leq \gamma. \tag{38}$$

WS and WT are the weighting functions for the tracking error and robust performances, respectively. The weighting function WS is a first-order low-pass filter used to achieve a proper tracking performance. Besides, the weighting function WT is a first-order high-pass filter used to obtain desired robust performances.

Equation (38) can be transformed into a linear matrix inequality (LMI) and numerically solved by LMI toolbox/MATLAB [37].

The graph of the singular values of the error conversion function to reference values, which is the same as the sensitivity function, along with the inverse of the performance weight function, is shown in Figure 5. As can be seen in the figure, the sensitivity function is located under the inverse graph of the performance weight function.

The diagram of the singular values of the output conversion function to the reference values, which is the sensitivity complement function, along with the inverse of the uncertain weight function, is shown in Figure 6. As can be seen in the figure, the sensitivity complement function is located under the inverse graph of the uncertain weight function.

The graph of the singular values of the product of the transformation function of the complement of the sensitivity in the uncertain weight function and the product of the transformation function of the sensitivity in the performance weight function is shown in Figure 7. As mentioned before and given in the definition of the mixed sensitivity method, robust stability is ensured by minimizing the H∞ norm weighted transformation function from Wr to ZT $W_T G_r K_r * (I + G_r K_r)_\infty^{-1} \leq 1$ and tracking and attenuation of disturbance by minimizing the H∞ norm function. The conversion from Wr to ZS can be achieved, $W_S(I + G_r K_r)^{-1}{}_\infty \leq 1$. As can be seen in the figure, both of these conditions have been achieved with the designed controller.

4. Kalman Filter

The Kalman filter is an optimal linear filter that affects state-space static and dynamic linear systems and provides an optimal estimation of the system states using its dynamic and reversible equations in the conditions where they are not accessible. The filter can also take into account the impact of all the system's previous and fundamental data in its estimations at each moment.

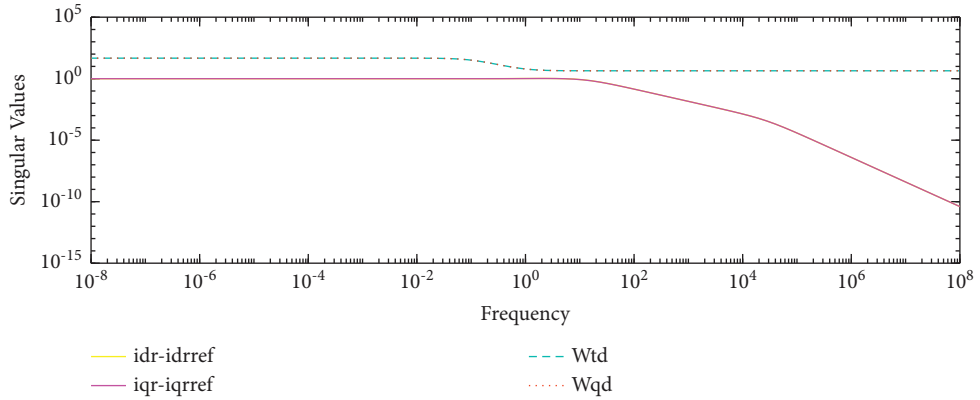

FIGURE 6: The sensitivity complement function and the inverse of the uncertain weight function.

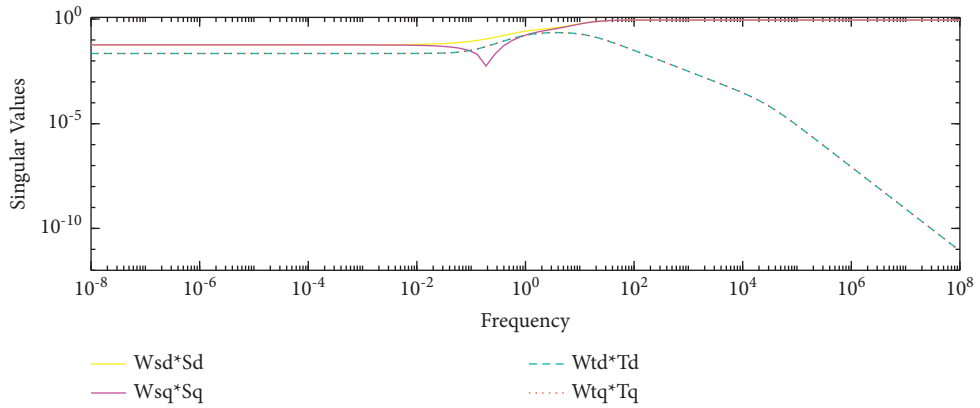

FIGURE 7: The product of the transformation function of the complement of the sensitivity in the uncertain weight function and the product of the transformation function of the sensitivity in the performance weight function.

If the mean square error of the estimation is minimized, this filter can provide excellent estimates of the past, present, and future states of the system [38,39]. To solve the constraint issue in the Kalman filter for linear systems, an EKF has been introduced to estimate the nonlinear system states. In fact, this filter estimates the nonlinear model as a time-varying linear model [40]; since the linearization of nonlinear system equations leads to the deviation of the mean error and covariance in the calculations and this deviation gradually gives rise to the estimated divergence in the recursive equations, a UKF is presented [41].

The state-space model of the discrete-time nonlinear system with respect to system noise is given as follows [40]:

$$\begin{aligned} x_{k+1} &= f\left(x_k.w_k.u_k\right), \\ z_k &= h\left(x_k.v_k\right). \end{aligned} \tag{39}$$

In this system, x_k is the state parameter, z_k is the measurement vector, and $w_k$and v_k are the process and measurement noises, respectively.

4.1. Extended Kalman Filter. The design method of the EKF system at the linearized and operating point is as follows [40]:

$$x_k = \hat{x}_{k|k-1} + A\left(x_{k-1} - \hat{x}_{k-1|k-1}\right) + W_{w_{k-1}}, \tag{40}$$

$$z_k = \tilde{Z}_k + H\left(x_k - \hat{x}_{k|k-1}\right) + V_{v_k}, \tag{41}$$

$$\tilde{z}_k = h\left(\hat{x}_{k|k-1}.0\right), \tag{42}$$

$$A_{[i,j]} = \frac{df_{[i]}}{dx_{[j]}}\left(\hat{x}_{k-1|k-1}.u_k.0\right), \tag{43}$$

$$W_{[i,j]} = \frac{df_{[i]}}{dw_{[j]}}\left(\hat{x}_{k-1|k-1}.u_k.0\right), \tag{44}$$

$$H_{[i,j]} = \frac{dh_{[i]}}{dx_{[j]}}\left(\hat{x}_{k|k-1}.0\right), \tag{45}$$

$$V_{[i,j]} = \frac{dh_{[i]}}{dv_{[j]}}\left(\hat{x}_{k|k-1}.0\right). \tag{46}$$

The EKF basis consists of two stages prediction and correction. The covariance and state estimates are used from the previous stage in the prediction stage.

$$\hat{x}_{k|k-1} = f\left(\hat{x}_{k-1|k-1}.u_k.0\right), \tag{47}$$

$$P_{k|k-1} = A_k P_{k-1|k-1} A_k^T + W_k Q_{k-1} W_k^T. \tag{48}$$

In the correction step, the covariance matrix and the measured state are modified.

$$K_k = P_{k|k-1} H_k^T \left(H_k P_{k|k-1} + V_k R_k V_k^T\right)^{-1}, \tag{49}$$

$$\hat{x}_{k|k} = \hat{x}_{k|k-1} + K_k\left(z_k - h\left(\hat{x}_{k|k-1}.0\right)\right), \tag{50}$$

$$P_{k|k} = (I - K_k H_k) P_{k|k-1}, \tag{51}$$

where Q_k and R_k are process and measurement noise covariance matrices, respectively.

4.2. Unscented Kalman Filter. The UKF is based on an unscented transform sampling technique that selects some sample points to estimate a possible model from the state level. These points are known as Sigma points. Like the EKF, the UKF design includes two stages of prediction and correction. In the prediction stage, some Sigma points are removed, and then the state and covariance matrices are calculated as the average weight of these points. To find the Sigma points, first, the state and covariance complemented by the mean and covariance of the process noise are estimated [41].

$$\begin{aligned} x_{k-1|k-1}^a &= \begin{bmatrix} \hat{x}_{k-1|k-1}^T & E\left[w_k^T\right] \end{bmatrix}^T, \\ P_{k-1|k-1}^a &= \begin{bmatrix} P_{k-1|k-1} & 0 \\ 0 & Q_k \end{bmatrix}. \end{aligned} \tag{52}$$

Then, 2L + 1 Sigma points are found by the following equations:

$$X_{k-1|k-1}^0 = x_{k-1|k-1}^a, \tag{53}$$

$$X_{k-1|k-1}^i = \begin{cases} x_{k-1|k-1}^a + \left(\sqrt{(L+\lambda)P_{k-1|k-1}^a}\right)_i, \\ i = 1....L \\ x_{k-1|k-1}^a + \left(\sqrt{(L+\lambda)P_{k-1|k-1}^a}\right)_{i-L}, \\ i = L+1....2L. \end{cases} \tag{54}$$

The Sigma points are obtained through the predicted state function, and the covariance is approximated using the weighted mean Sigma points from the previous step.

$$X_{k|k-1}^i = f\left(X_{k-1|k-1}^i\right), \tag{55}$$

$$\tilde{x}_{k|k-1} = \sum_{i=0}^{2L} W_s^i X_{k|k-1}^i, \tag{56}$$

$$P_{k|k-1} = \sum_{i=0}^{2L} W_c^i \left[X_{k|k-1}^i - \tilde{x}_{k|k-1}\right]\left[X_{k|k-1}^i - \tilde{x}_{k|k-1}\right]^T. \tag{57}$$

The weight functions can be obtained as follows:

$$W_s^0 = \frac{\lambda}{\lambda + L}, \tag{58}$$

$$W_c^0 = \frac{\lambda}{\lambda + L} + \left(1 - \alpha^2 + \beta\right), \tag{59}$$

$$W_s^0 = W_c^i = \frac{1}{2(\lambda + L)}, \tag{60}$$

$$\lambda = \alpha^2 (L + \kappa) - L, \tag{61}$$

where β corresponds to the distribution of X. α and K are associated with Sigma points, in which α is usually a small positive value (e.g., 0.001), and K is usually chosen near zero.

Next, the predicted state and covariance complemented by the mean and covariance of the measured noise are updated. After that, 2L + 1 Sigma points are extracted from the completed state and covariance.

$$x_{k|k-1}^a = \begin{bmatrix} \hat{x}_{k|k-1}^T & E\left[v_k^T\right] \end{bmatrix}^T, \tag{62}$$

$$P_{k|k-1}^a = \begin{bmatrix} P_{k|k-1} & 0 \\ 0 & R_k \end{bmatrix}, \tag{63}$$

$$X_{k|k-1}^0 = x_{k|k-1}^a, \tag{64}$$

$$X_{k|k-1}^i = \begin{cases} x_{k|k-1}^a + \left(\sqrt{(L+\lambda)P_{k|k-1}^a}\right)_i, \\ i = 1....L \\ x_{k|k-1}^a + \left(\sqrt{(L+\lambda)P_{k|k-1}^a}\right)_{i-L}, \\ i = L+1....2L. \end{cases} \tag{65}$$

Sigma points are predicted using the function and the measurement parameters. Meanwhile, the covariance of the measurement is obtained by the weighted average of Sigma points.

$$\gamma_k^i = f\left(X_{k|k-1}^i\right), \tag{66}$$

$$\tilde{z}_{k|k-1} = \sum_{i=0}^{2L} W_s^i \gamma_k^i. \tag{67}$$

The predicted covariance matrix and the measurement mode are used to obtain the gain of the Kalman filter.

$$K_k = P_{x_k z_k} {P_{z_k z_k}}^{-1}, \tag{68}$$

$$P_{z_k z_k} = \sum_{i=0}^{2L} W_c^i \left[\gamma_k^i - \tilde{z}_{k|k-1}\right]\left[\gamma_k^i - \tilde{z}_{k|k-1}\right]^T, \tag{69}$$

$$P_{x_k z_k} = \sum_{i=0}^{2L} W_c^i \left[x_{k|k-1}^i - \tilde{x}_{k|k-1}\right]\left[\gamma_k^i - \tilde{z}_{k|k-1}\right]^T. \tag{70}$$

The state and covariance matrices are updated using the following equations:

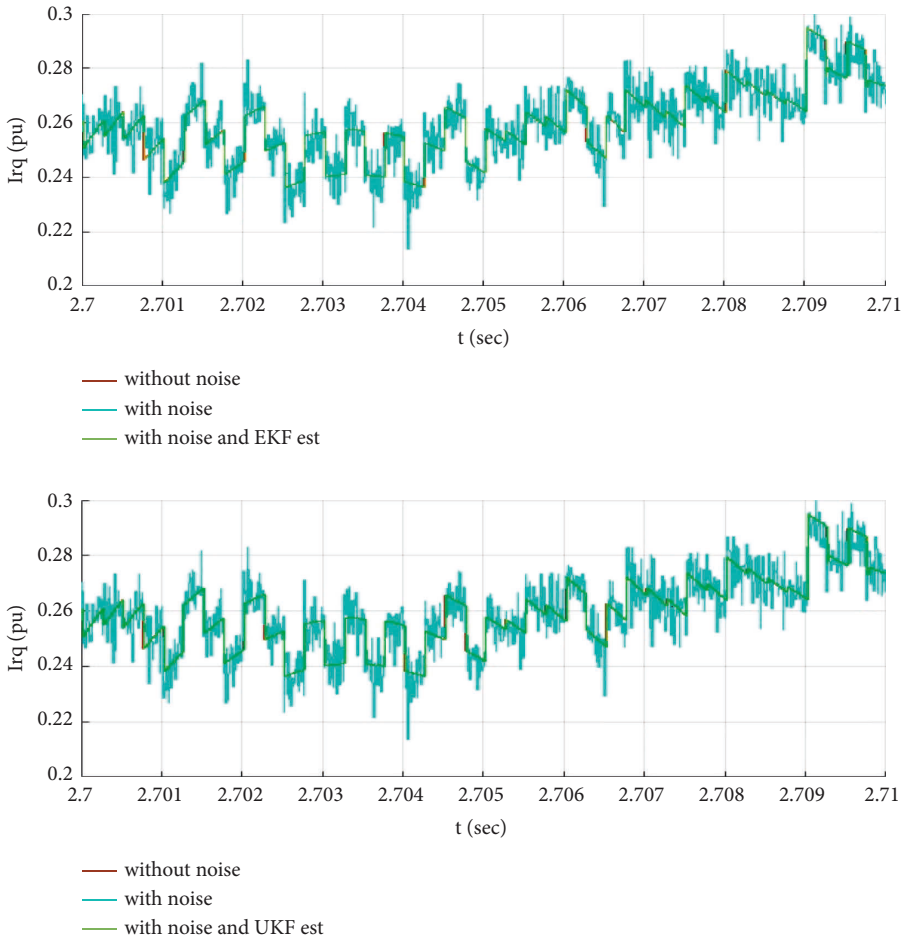

Figure 8: The comparison of estimations obtained by the EKF and UKF for I_{rq}.

$$\tilde{x}_{k|k} = \tilde{x}_{k|k-1} - K_k(z_k - \tilde{z}_k), \tag{71}$$

$$P_{k|k} = P_{k|k-1} - K_k P_{z_k z_k} K_k^T. \tag{72}$$

4.3. The Application of Kalman Filter to the DFIG. Using the above-mentioned assumptions, the state-space model matrices of the DFIG system will be derived as follows to obtain step matrices of the Kalman filter:

$$f = \begin{pmatrix} -\left(\frac{a+1}{T_r} + \frac{a}{T_s}\right)x_1 + (\omega_s - \omega_m)x_2 + \left(\frac{a}{L_m T_s}\right)x_3 + \left(-\frac{a\omega_m}{L_m}\right)x_4 - \left(\frac{a}{L_m}\right)u_1 + \left(\frac{1}{\sigma L_r}\right)u_3 \\ -(\omega_s - \omega_m)x_1 - \left(\frac{a+1}{T_r} + \frac{a}{T_s}\right)x_2 + \left(\frac{a\omega_m}{L_m}\right)x_3 + \left(\frac{a}{L_m T_s}\right)x_4 - \left(\frac{a}{L_m}\right)u_2 + \left(\frac{1}{\sigma L_r}\right)u_4 \\ \left(\frac{L_m}{T_s}\right)x_1 - \left(\frac{1}{T_s}\right)x_3 + (\omega_s)x_4 + u_1 \\ \left(\frac{L_m}{T_s}\right)x_2 - (\omega_s)x_3 - \left(\frac{1}{T_s}\right)x_4 + u_2 \end{pmatrix} h = \begin{pmatrix} x_1 \\ x_2 \\ -\left(\frac{L_m}{L_s}\right)x_1 + \left(\frac{1}{L_s}\right)x_3 \\ -\left(\frac{L_m}{L_s}\right)x_2 + \left(\frac{1}{L_s}\right)x_4 \end{pmatrix}. \tag{73}$$

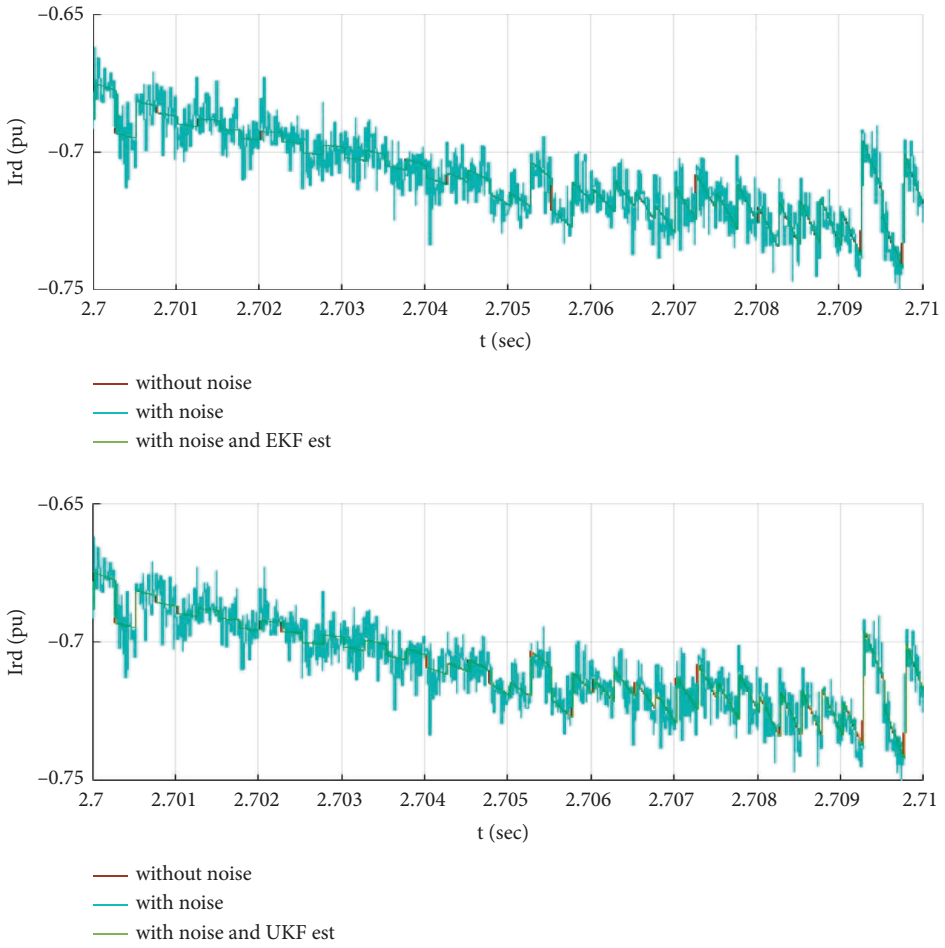

Figure 9: The comparison of estimations obtained by the EKF and UKF for I_{rd}.

As described in the previous equations, the EKF matrices will be as follows:

$$A = \begin{bmatrix} -\left(\frac{a+1}{T_r} + \frac{a}{T_s}\right) & (\omega_s - \omega_m) & \frac{a}{L_m T_s} & -\frac{a\omega_m}{L_m} \\ -(\omega_s - \omega_m) & -\left(\frac{a+1}{T_r} + \frac{a}{T_s}\right) & \frac{a\omega_m}{L_m} & \frac{a}{L_m T_s} \\ \frac{L_m}{T_s} & 0 & -\frac{1}{T_s} & \omega_s \\ \frac{L_m}{T_s} & -\omega_s & -\frac{1}{T_s} & \end{bmatrix}, \quad (74)$$

$$H = \begin{bmatrix} 1 & 0 & 0 & 0 \\ 0 & 1 & 0 & 0 \\ -\frac{L_m}{L_s} & 0 & \frac{1}{L_s} & 0 \\ 0 & -\frac{L_m}{L_s} & 0 & \frac{1}{L_s} \end{bmatrix}.$$

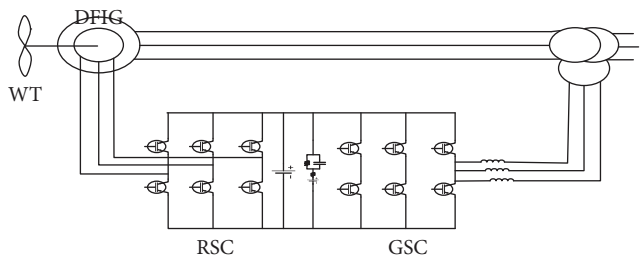

Figure 10: The layout of the simulated system.

Table 2: Parameters of the simulated machine.

Rated power of the machine	1.5 MW
Stator voltage	575 V
Stator resistance	0.00706 pu
Rotor resistance	0.005 pu
Mutual inductance	2.9 pu
Stator inductance	3.071 pu
Rotor inductance	3.056 pu

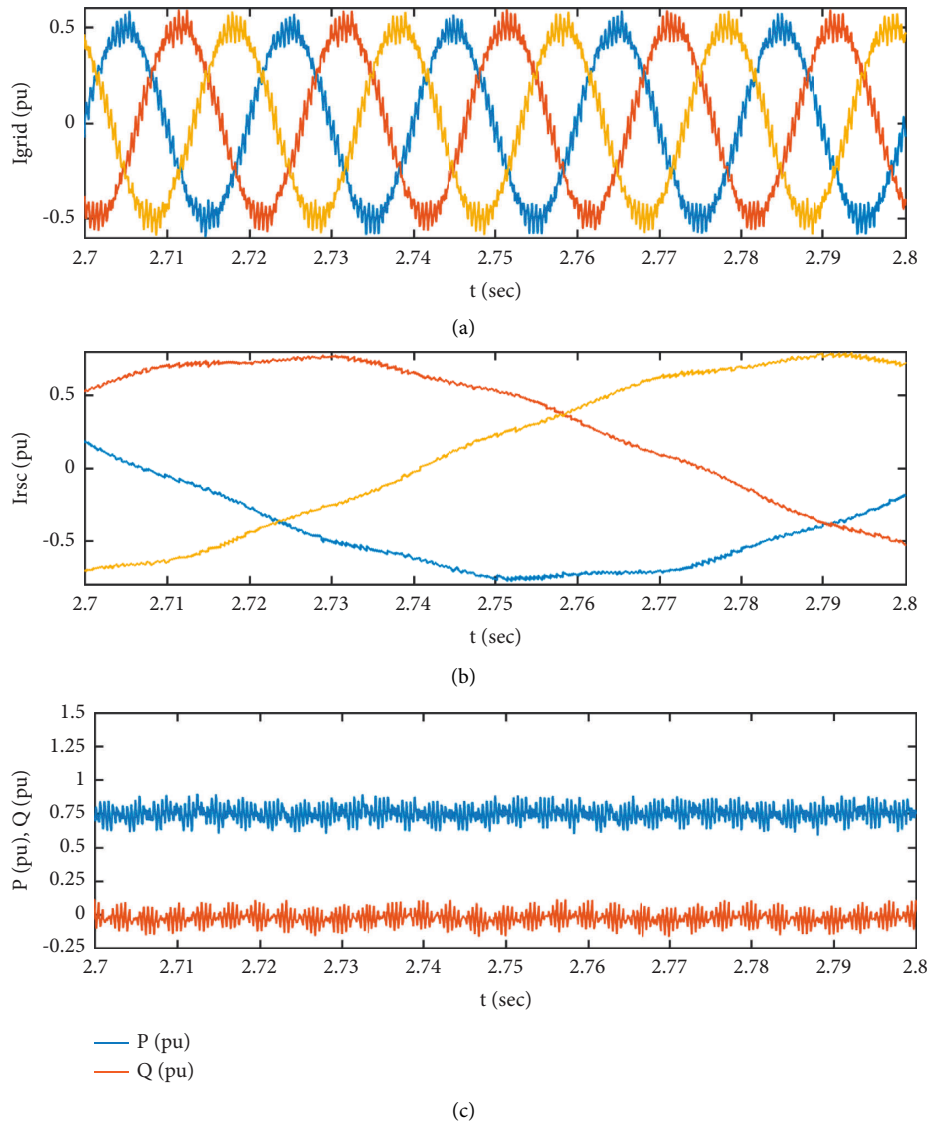

Figure 11: The simulation results when the rotor speed is 0.9 pu with the rated values for machine parameters. (a) Grid current, (b) rotor side converter current, and (c) grid active and reactive power.

To have a more realistic simulation, measurement noise is added to the system. First, prior to system simulation based on the model uncertainty, the outputs of the system and the rotor currents are simulated using both EKF and UKF methods, considering the measurement noise. The results of this section along with the most efficient methods will be used in system simulation with model and measurement uncertainty.

The simulation results of obtained rotor currents using EKF and UKF methods with and without measurement noise are shown in Figures 8 and 9. In both estimation methods, the results show that the measurement noise is eliminated, and the signal approaches the noise-free mode. We will use the UKF method to deactivate the measured noise in the next step, where we will simulate the system with the robust controller. Both methods are able to eliminate the system noise considering the fact the model uses a linear system. However, for the UKF selection, it has been assumed that nonmodeled and nonlinear modes are possible in the actual state of the system, so there is a possibility of its occurrence, and the types of uncertainties applied in the simulation stage, the combination of which exacerbates the nonlinearity of the system.

5. Simulation Results

Simulations have been implemented in the MATLAB software environment. Figure 10 illustrates the layout of the simulated system. In the simulation process, the model available in MATLAB was used for modeling the DFIG system. The rated power of the induction machine is 1.5 MW, and the link voltage is 1200 V DC. The parameters listed in Table 2 were exploited for modeling the machine [27].

In the first step of simulations, the machine parameters are set to their rated values. The rotor speed during the simulations was set in three states in fixed values equal to 0.9,

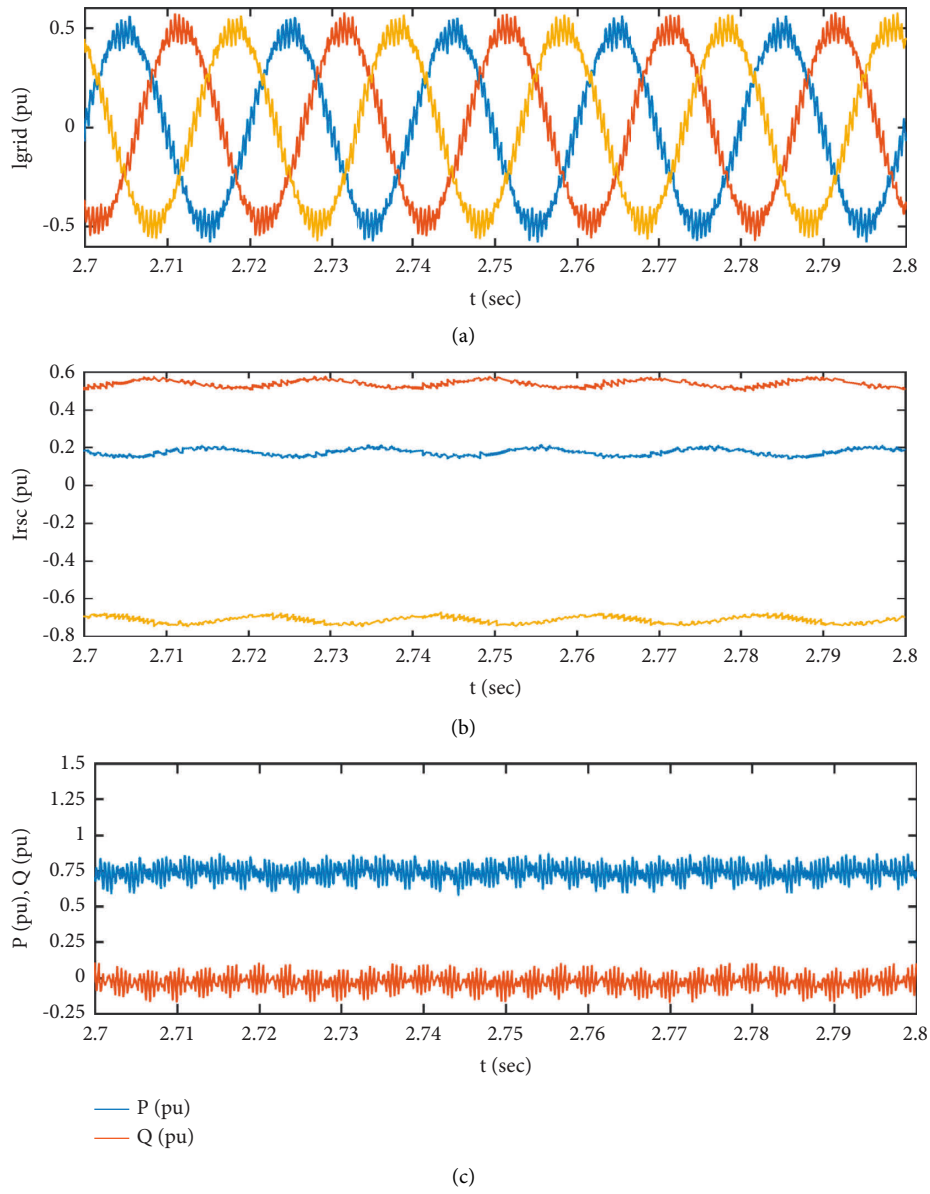

Figure 12: The simulation results when the rotor speed is 1 pu with the rated values for machine parameters. (a) Grid current, (b) rotor side converter current, and (c) grid active and reactive power.

1, and 1.2 pu. According to the topology used here, one of the main purposes of the controller design with mixed sensitivity approach is to keep the power injected into the grid constant by exchanging battery energy in DC link and DFIG in different turbine speed modes (synchronous speed, subsynchronous speed, and supersynchronous speed); therefore, the rotor speed is displayed to show the controller operation for turbine power changes in different turbine speed modes. The simulation results for these values are given inFigures 11–13, respectively.

In the next step of simulations, the stator and rotor resistances and the mutual inductance are varied, and their values increase up to 25% [34–36, 42, 43]. The rotor speed is 0.9 pu during the simulation. The simulation results for these values are shown in Figure 14. Finally, in the last step of simulations, the values of stator and rotor resistances and mutual inductance are varied, and their values decrease up to 25% at this time [34–36, 42, 43]. The rotor speed is fixed at 1.2 pu during the simulation process. The simulation results for this case are represented in Figure 15.

Figures 11–15 show the simulation results for the rated case and for increased and decreased values of the stator and rotor resistances and mutual inductance from their rated values. In the proposed controller design, the mixed sensitivity method with a multiobjective cost function is used, and this function fulfills the design objective in nominal performance, proper tracking, perturbation attenuation, and robust stability. Therefore, in order to realize this cost function and show robust performance and stability, the system has been simulated in different modes of turbine speed and uncertainties. In all the cases, it is observed that the injected power to the grid has been maintained at a

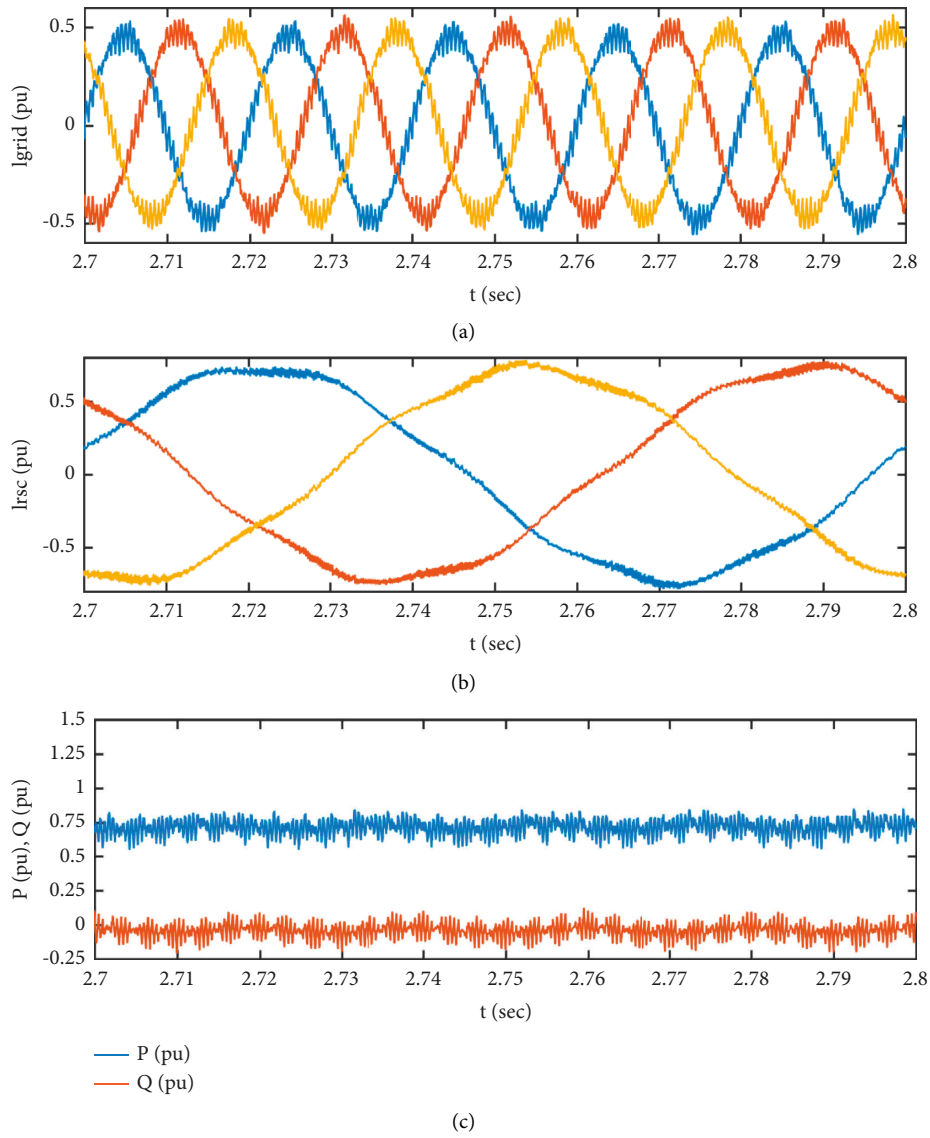

FIGURE 13: The simulation results when the rotor speed is 1.2 pu with the rated values for machine parameters. (a) Grid current, (b) rotor side converter current, and (c) grid active and reactive power.

constant value of 0.75 pu. The reference grid power can be selected as the average power supplied by the wind turbine to supply constant power to the grid during the entire operation period. Hence, the 0.75 pu grid power reference is selected, which is one of the objectives of the mixed sensitivity cost function and keeps the output power constant at 0.75 pu. Considering that the designed controller is a robust controller and according to the comparisons between figures, when uncertainty is applied to the system and the system parameters are changed, the system continues its perfect performance using the designed controller. This verifies that when the system deviates from its rated values, the performance of the controller is not affected, which means that the system with the designed controller has stable and robust performance. Therefore, the optimal design objectives have been achieved through the mixed sensitivity method with the nominal performance of the system in the nominal values of the system parameters, the robust performance and stability of the system in different uncertainties, and proper tracking by keeping the output power of the system constant.

Figure 16 compares the system response with the H_∞ control approach and classic voltage-oriented (VC). The grid power for the H_∞ control is maintained constant at the reference value, whereas the grid power does not track the reference value and the PI controller depends on the parameters. In both methods, VC is used to design the controller. The only difference is that, in the classical vector controller, the PI controller is used in the internal current loop, and in the robust controller, the H_∞ controller is used. Reference powers are used to generate reference currents, either from machine relationships or from PI controllers. To show the robustness of the designed controller, the first method, which depends on the parameters of the machine, is

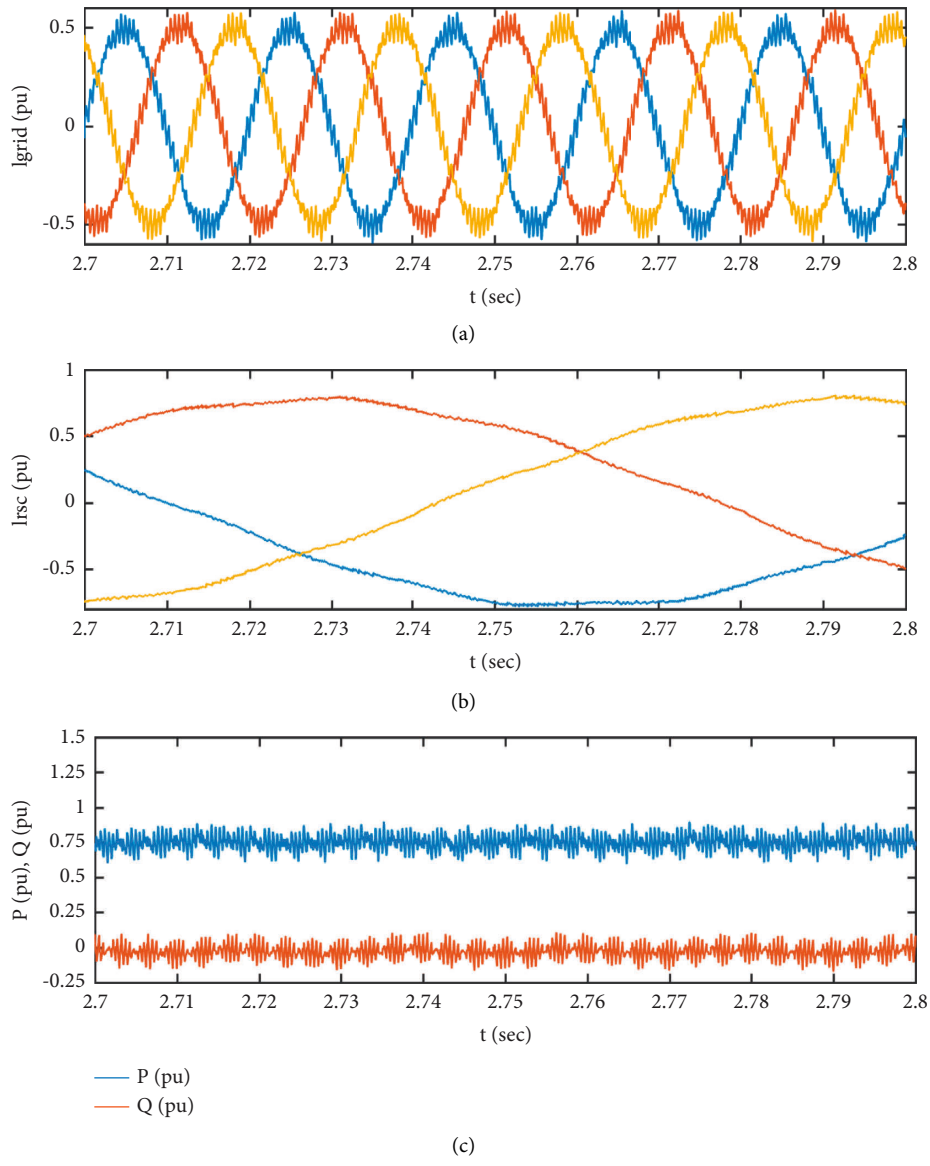

Figure 14: The simulation results when the rotor speed is 0.9 pu and the values of stator and rotor resistances and mutual inductance have increased by 25% above their rated values. (a) Grid current, (b) rotor side converter current, and (c) grid active and reactive power.

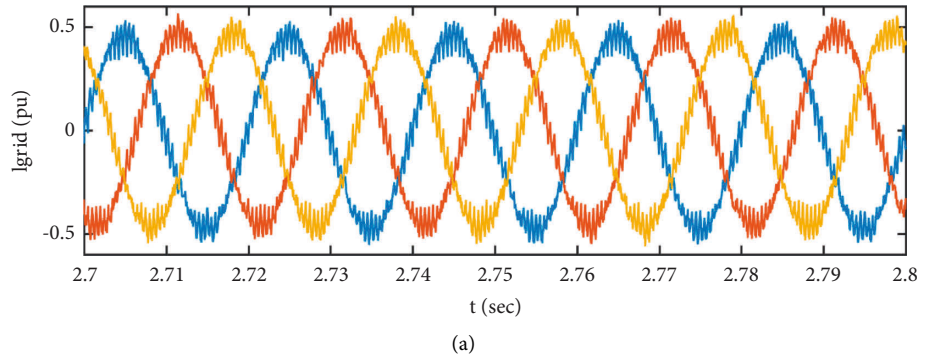

Figure 15: Continued.

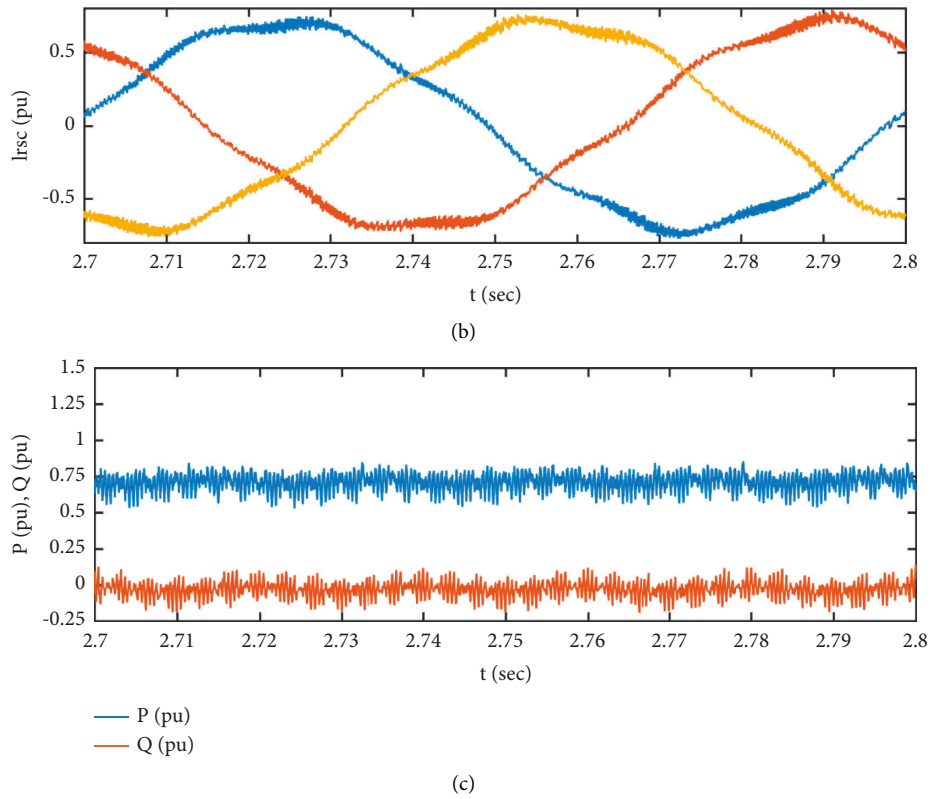

FIGURE 15: The simulation results when the rotor speed is 0.9 pu and the values of stator and rotor resistances and mutual inductance have decreased by 25% above their rated values. (a) Grid current, (b) rotor side converter current, and (c) grid active and reactive power.

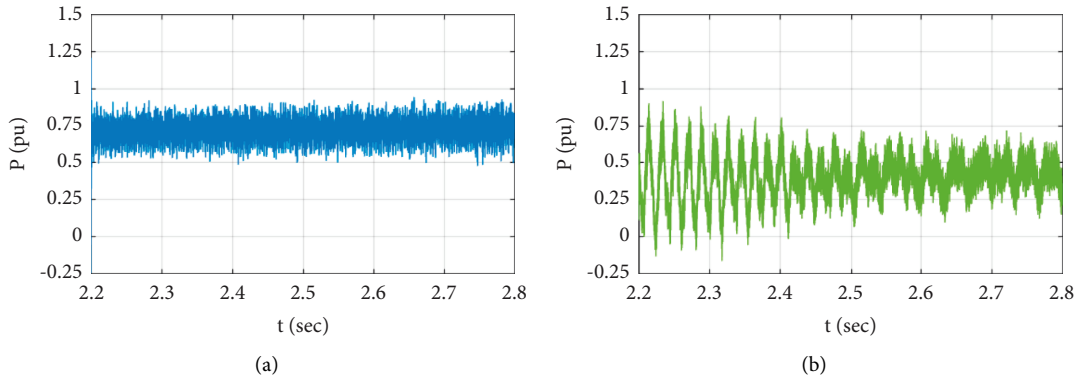

FIGURE 16: The comparison of system responses with H∞ control and PI control and the values of stator and rotor resistances and mutual inductance have decreased by 50% under their rated values [34, 35, 42, 43]. (a) H_∞ controller and (b) PI controller.

used. The comparison of the results shows that the classical vector controller depends on the parameters of the system, and by deviating their values, the stability and performance of the system are lost, while in the robust controller with the mixed sensitivity approach, the desired performance and stability are obtained.

6. Conclusion

The paper presents a robust control method based on the H_∞ controller in the presence of model and measurement uncertainties for a DFIG with a topology that uses a storage battery in the DC link to maintain the injected power to the grid at a constant value. In designing the robust controller, uncertainty is considered a parametric uncertainty. The proposed method makes use of a robust H_∞ controller in the current control loop of the RSC to make the system robust against the variations in the machine parameters. The Kalman filter method is used to inactivate measurement noises in the parameters used in the controller. The simulation results show that, despite the variations in the system parameters and measurement noises, it is able to continue its

desired operation and inject constant power into the grid. Moreover, the designed controller presents a robust performance against the change of parameters and measurement uncertainties. In all the cases, it is observed that the injected power to the grid has been maintained at a constant value of 0.75 pu. A comparison between the system responses obtained by the PI control and H_∞ control shows that the grid power maintains its stability at the reference value when the H_∞ control is used, whereas the grid power is not controlled when using the PI method, and it depends on the PI parameters.

Symbols

V_{qs}, V_{ds}: Stator voltage on q and d axes
V_{qr}, V_{dr}: Rotor voltage on q and d axes
i_{qs}, i_{ds}: Stator currents on q and d axes
i_{qr}, i_{dr}: Rotor currents on q and d axes
ω_s: Synchronous speed
ω_m: Rotor speed
λ_{qs}, λ_{ds}: Stator fluxes on q and d axes
λ_{qr}, λ_{dr}: Rotor fluxes on q and d axes
R_s: Stator resistance
R_r: Rotor resistance
L_s: Self-inductances of the stator
L_r: Self-inductances of the rotor
L_m: Mutual inductance
P_s: Active output power of the stator
Q_s: Reactive output power of the stator
X: State vector
U: Input vector
Y: Output vector
$\overline{R}_s$: Rated values of stator resistance
$\overline{R}_r$: Rated values of rotor resistance
k_{R_s}: Uncertainty relationships with their corresponding parameter
k_{R_r}: Uncertainty relationships with their corresponding parameter
k_{ω_m}: Uncertainty relationships with their corresponding parameter
$s\delta_{R_s}$, δ_{R_r}, δ_{ω_m}: Arbitrary numbers subject to $|\delta_{R_s}.\delta_{R_r}.\delta_{\omega_m}| \le 1$
$\widetilde{W}_W$: Input signal of the disturbance channel
$\widetilde{Z}_W$: Output signal of the disturbance channel
$W_r = \left[V_{ds} \;\; V_{qs} \;\; i_{dr}^{\text{ref}} \;\; i_{qr}^{\text{ref}}\right]^T$: External control input
$V_r = \left[V_{dr} \;\; V_{qr}\right]^T$: Controller output
$e_r = \left[e_{dr} \;\; e_{qr}\right] = \left[i_{dr}^{ref} - i_{dr} \;\; i_{qr}^{ref} - i_{qr}\right]^T$: Controller input
:
i_{qr}^{ref} i_{dr}^{ref}: Reference rotor currents on q and d axes
W_S, W_T: Weighting functions
G_r: the realization of the state space
K_r: H_∞ robust controller
x_k: State parameter at time step k
z_k: Measurement vector at time step k
w_k: Process noises at time step k
v_k: Measurement noises at time step k
$\hat{x}_k$: Posterior estimate of the state (from a previous time step k)
$A_{[i,j]}$: The Jacobian matrix of partial derivatives of f with respect to x
$W_{[i,j]}$: The Jacobian matrix of partial derivatives of f with respect to w
$H_{[i,j]}$: The Jacobian matrix of partial derivatives of H with respect to x
$V_{[i,j]}$: The Jacobian matrix of partial derivatives of H with respect to v
P_k: Covariance matrices at time step k
Q: Process noise covariance matrices
R: Measurement noise covariance matrices
Q_k: Process noise covariance matrices at time step k
R_k: Measurement noise covariance matrices at time step k
β: Corresponds to the distribution of X
αK: Associated with Sigma points
X_{k-1}^i: Prior estimate of the state (from a previous time step $k-1$).

Data Availability

The data used to support the findings of this study can be obtained from the corresponding author upon request.

Conflicts of Interest

The authors declare that there are no conflicts of interest regarding the publication of this article.

References

[1] R. Pena, J. C. Clare, and G. M. Asher, "Doubly fed induction generator using back-to-back PWM converters and its application to variable-speed wind-energy generation," *IEE Proceedings - Electric Power Applications*, vol. 143, no. 3, pp. 231–241, 1996.
[2] J. b. Hu and Y. k. He, "Dynamic modelling and robust current control of wind-turbine driven DFIG during external AC

voltage dip," *Journal of Zhejiang University - Science*, vol. 7, no. 10, pp. 1757–1764, 2006.

[3] J. Hu, Y. He, L. Xu, and B. W. Williams, "Improved control of DFIG systems during network unbalance using PI–R current regulators," *IEEE Transactions on Industrial Electronics*, vol. 56, no. 2, pp. 439–451, 2009.

[4] L. Xu and P. Cartwright, "Direct active and reactive power control of DFIG for wind energy generation," *IEEE Transactions on Energy Conversion*, vol. 21, no. 3, pp. 750–758, 2006.

[5] F. K. Moghadam, S. Ebrahimi, A. Oraee, and J.M. Veln, "Vector control optimization of DFIGs under unbalanced conditions," *International Transactions on Electrical Energy Systems*, vol. 28, p. e2583, 2018.

[6] Z. Xin-fang, X. Da-ping, and L. Yi-bing, "Predictive functional control of a doubly fed induction generator for variable speed wind turbines," *IEEE World Congress on Intelligent Control and Automation*, vol. 4, pp. 3315–3319, 2004.

[7] J. Morren, S. DeHaan, and W. H. de Haan, "Ride through of wind turbines with doubly-fed induction generator during a voltage dip," *IEEE Transactions on Energy Conversion*, vol. 20, pp. 435–441, 2005.

[8] J. Guo, X. Cai, and Y. Gong, "Decoupled control of active and reactive power for a grid-connected doubly-fed induction generator," in *Proceeding. if the Conf. Electric Utility Deregulation and Restructuring and Power Technologies (DRPT)*, IEEE, Nanjing, China, 2008.

[9] X. Yao, Y. Jing, and Z. Xing, "Direct torque control of a doubly-fed wind generator based on grey-fuzzy logic," in *Proceeding. if the. Int. Conf. Mechatronics and Automation (ICMA)*, IEEE, Nanjing, China, 2007.

[10] J. Hu, Y. Li, and J. Zhu, "Multi-objective model predictive control of doubly-fed induction generators for wind energy conversion," *IET Generation, Transmission & Distribution*, vol. 13, no. 1, pp. 21–29, 2018.

[11] G. Abad, M. A. Rodriguez, and J. Poza, "Two-level VSC-based predictive direct power control of the doubly fed induction machine with reduced power ripple at low constant switching frequency," *IEEE Transactions on Energy Conversion*, vol. 23, no. 2, pp. 570–580, 2008.

[12] Y. Sahri, S. Tamalouzt, F. Hamoudi et al., "New intelligent direct power control of DFIG-based wind conversion system by using machine learning under variations of all operating and compensation modes," *Energy Reports*, vol. 7, pp. 6394–6412, 2021.

[13] D. D. Trivedi, U. B. Bhatt, and S. C. Vora, "Application of EKF based dynamic state estimation for DFIG rotor power control uunder faulty current," *International Journal of Advanced Research in Engineering & Technology*, vol. 8, no. 4, pp. 95–110, 2017.

[14] M. Hadipour, M. R. Alizadeh Pahlavani, and H. Meyar Naim, "Application of kalman filter for parameter estimation of doubly-fed induction generators in wind turbine systems," *Majlesi Journal of Energy Management*, vol. 5, no. 2, 2016.

[15] A. Boussoufa, M. Kidouche, and A. Ahriche, "Rotor speed and flux estimation of a doubly-fed induction machine using extended kalman filter," *Algerian Journal of Signals and Systems*, vol. 2, no. 4, pp. 266–273, 2017.

[16] S. Yu, K. Emami, T. Fernando, H. H. C. Iu, and K. P. Wong, "State estimation of doubly fed induction generator wind turbine in complex power systems," *IEEE Transactions on Power Systems*, vol. 31, no. 6, pp. 4935–4944, 2016.

[17] D. Zhi and L. Xu, "Direct power control of DFIG with constant switching frequency and improved transient performance," *IEEE Transactions on Energy Conversion*, vol. 22, no. 1, pp. 110–118, 2007.

[18] R. F. Nayeh, H. Moradi, and G. Vossoughi, "Multivariable robust control of a horizontal wind turbine under various operating modes and uncertainties: a comparison on sliding mode and H∞ control," *International Journal of Electrical Power & Energy Systems*, vol. 115, Article ID 105474, 2020.

[19] B. E. Sedhom, A. Y. Hatata, M. M. El-Saadawi, and E. E. Abd-Raboh, "Robust adaptive H-infinity based controller for islanded microgrid supplying non-linear and unbalanced loads," *IET Smart Grid*, vol. 2, no. 3, pp. 420–435, 2019.

[20] Y. J. Isbeih, M. S. El Moursi, W. Xiao, and E. El-Saadany, "H_∞ mixed-sensitivity robust control design for damping low-frequency oscillations with DFIG wind power generation, IET Generation," *IET Generation, Transmission & Distribution*, vol. 13, no. 19, pp. 4274–4286, 2019.

[21] K. R. Suraparaju and G. Pillai, "Type 2 fuzzy logic-based robust control strategy for power sharing in microgrids with uncertainties in operating conditions," *International Transactions on Electrical Energy Systems*, vol. 27, no. 4, p. e2294, 2017.

[22] Z. Ortatepe and A. Karaarslan, "Robust predictive sensorless control method for doubly fed induction generator controlled by matrix converter," *International Transactions on Electrical Energy Systems*, vol. 30, no. 12, Article ID e12650, 2020.

[23] S. R. Aali, M. R. Besmi, and M. H. Kazemi, "Adaptive filtering with robust controller for improvement of inertial response of wind turbine," *International Transactions on Electrical Energy Systems*, vol. 29, no. 10, Article ID e12089, 2019.

[24] A. Kasbi and A. Rahali, "Adaptive FOPI controller based on the fuzzy supervisory for wind power conversion system equipped by a doubly fed induction generator," *International Transactions on Electrical Energy Systems*, vol. 31, no. 8, Article ID e12923, 2021.

[25] S. Tamalouzt, Y. Belkhier, Y. Sahri et al., "Enhanced direct reactive power control-based multi-level inverter for DFIG wind system under variable speeds," *Sustainability*, vol. 13, no. 16, p. 9060, 2021.

[26] S. Tamalouzt, Y. Belkhier, Y. Sahri, N. Ullah, R. N. Shaw, and M. Bajaj, "New direct reactive power control based fuzzy and modulated hysteresis method for micro-grid applications under real wind speed," *Energy Sources, Part A: Recovery, Utilization, and Environmental Effects*, vol. 44, no. 2, pp. 4862–4887, 2022.

[27] V. C. Ganti, B. Singh, S. K. Aggarwal, and T. C. Kandpal, "DFIG-based wind power conversion with grid power leveling for reduced gusts," *IEEE Transactions on Sustainable Energy*, vol. 3, no. 1, pp. 12–20, 2012.

[28] P. C. Krause, O. Wasynczuk, S. D. Sudhoff, and S. D. Pekarek, *Analysis of Electric Machinery and Drive Systems*, John Wiley & Sons, New York USA, 2013.

[29] K. Zhou and J. C. Doyle, *Essentials of Robust Control*, Prentice-Hall, Upper Saddle River, NJ, 1998.

[30] S. Skogestad and I. Postlethwaite, *Multivariable Feedback Control Analysis and Design*, John Wiley & Sons, NY, 2001.

[31] C. Scherer, *Theory of Robust Control*, Delft University of Technology, Netherlands, Europe, 2001.

[32] J. Doyle, "Robust and optimal control," in *Proceedings of the 35th IEEE Conference on Decision and Control*, IEEE, New York USA, 1996.

[33] D. W. Gu, P. Petkov, and M. M. Konstantinov, *Robust Control Design with MATLAB®*, Springer Science & Business Media, Berlin, Germany, 2005.

[34] A. Abdelbaset, A. M. El-Sayed, and A. E. H. Abozeid, "Grid synchronisation enhancement of a wind driven DFIG using adaptive sliding mode control," *IET Renewable Power Generation*, vol. 11, no. 5, pp. 688–695, 2017.

[35] S. Ebrahimkhani, "Robust fractional order sliding mode control of doubly-fed induction generator (DFIG)-based wind turbines," *ISA Transactions*, vol. 63, pp. 343–354, 2016.

[36] A. Merabet, H. Eshaft, and A. A. Tanvir, "Power-current controller based sliding mode control for DFIG-wind energy conversion system," *IET Renewable Power Generation*, vol. 12, no. 10, pp. 1155–1163, 2018.

[37] P. Gahinet, A. Nemirovski, A. J. Laub, and M. Chilali, *LMI Control Toolbox for Use with MATLAB*, The Mathworks Inc, Natick, MA, 2000.

[38] G. Welch and G. Bishop, "An Introduction to the Kalman Filter," 2004, https://perso.crans.org/club-krobot/doc/kalman.pdf.

[39] H. W. Sorenson, *Kalman Filtering, Theory and Application*, IEEE, New Jersey, USA, 1985.

[40] E. A. Wan and A. T. Nelson, "Removal of noise from speech using the dual EKF algorithm," *International Conference on Acoustics, Speech, and Signal Processing*, IEEE, New Jersey, USA, 1988.

[41] S. Julier and J. Uhlmann, "A new extension of the Kalman lter to nonlinear systems," *Int.Symp. Aerospace/Defense Sensing, Simul. And Controls*, vol. 3068, pp. 182–219, 1997.

[42] S. Boubzizi, H. Abid, A. El hajjaji, and M. Chaabane, "Comparative study of three types of controllers for DFIG in wind energy conversion system," *Protection and Control of Modern Power Systems*, vol. 3, no. 1, p. 21, 2018.

[43] S. Z. Chen, N. C. Cheung, K. C. Wong, and J. Wu, "Grid synchronization of doubly-fed induction generator using integral variable structure control," *IEEE Transactions on Energy Conversion*, vol. 24, no. 4, pp. 875–883, 2009.